

# Physical properties of cement composites designed for aerostatic bearings

T. H. Panzera · P. H. R. Borges ·  
J. Campos Rubio · C. R. Bowen ·  
W. L. Vasconcelos

Received: 14 December 2007 / Accepted: 8 July 2008 / Published online: 17 July 2008  
© RILEM 2008

**Abstract** This paper investigates the physical properties of cement composites based on ordinary Portland cement (OPC) and silica particles as a potential material for porous aerostatic bearings for precision engineering applications. A full factorial design ( $2^{2 \times 4^1}$ ) was carried out to study the effects of silica properties (size and geometry) and uniaxial pressure (10 and 30 MPa) on the composite properties, namely bulk density, apparent porosity and intrinsic permeability of the ceramic composites. Scatter graphs were plotted to identify the existence of significant correlations between parameters. The cementitious composite manufactured with small

silica particles, non-spherical shape and low level of compaction pressure exhibited the most appropriate properties for the proposed application. In addition, mathematical models obtained from the response-correlation plots are potentially important tools for the development and design of new composites for porous bearing applications.

**Keywords** Cementitious composites · Aerostatic porous bearings · Mechanical properties · Full experimental design, precision engineering

---

T. H. Panzera (✉) · J. Campos Rubio  
Department of Mechanical Engineering, Federal  
University of Minas Gerais (UFMG), Av. Antônio Carlos  
6627, Campus Pampulha, 31 270 901 Belo Horizonte,  
MG, Brazil  
e-mail: tuliopanzera@hotmail.com

P. H. R. Borges  
Department of Engineering Materials, University of  
Sheffield, Sir Robert Hadfield Building, Mappin Street,  
Sheffield S1 3JD, UK

C. R. Bowen  
Materials Research Centre, Department of Mechanical  
Engineering, University of Bath, Bath BA2 7AY, UK

W. L. Vasconcelos  
Department of Metallurgical and Materials Engineering,  
Federal University of Minas Gerais (UFMG), Belo  
Horizonte, MG, Brazil

## 1 Introduction

Aerostatic bearings exhibit a number of advantages for precision engineering applications, namely: a small variation in properties with temperature, high damping, high operational speeds, limited wear and a capacity to support radial, axial and multi-axial loadings [1]. Aerostatic bearings employ a thin film of high-pressure air to support a load. Since air has a low viscosity the bearing gap needs to be thin, typically 1–10  $\mu\text{m}$  in thickness. All air bearings operate on the principle of supporting a load on a thin film of high pressure air which flows continuously out of the bearing and into the atmosphere [2]. Air bearings are typically classed as ‘orifice’ or ‘porous media’ types. In orifice bearings the pressurized air reaches at the bearing surface through a series of precisely sized holes which are produced by



machining. The use of a porous material as the bearing surface has the potential to create a highly uniform pressure distribution, as well as improved load capacity and stiffness. However, it is essential that the large numbers of minute restrictors in the porous bearing are uniformly distributed over the entire bearing surface. Typically, aerostatic air bearings provide improved accuracy of up to two orders of magnitude better than that of conventional rolling element bearings [3, 4].

It is well known that aerostatic bearings using material porosity as flow restrictors over the entire bearing surface provide significant advantages over bearings with conventional restrictors, which include improved load and stiffness characteristics along with simplicity in the bearing construction [5]. However, their widespread application in precision engineering has been hampered by the difficulties in predicting the fluid flow characteristics of porous materials [6], as well as stability problems believed to be related to the void volume between pores at the bearing surface [7].

Most porous materials used in aerostatic bearing applications are produced by partial sintering of powders, the most common materials being of graphite, ceramic or bronze. The permeability of a porous material is largely isotropic and since a machined bearing surface is somewhat granular in nature, its roughness value  $R_t$  approaches the size of the powders [8, 9]. The main requirements of a material for application as a porous aerostatic bearing are that the porosity level is between 20% and 35%, permeability coefficient between  $3.1 \times 10^{-15}$  to  $8.4 \times 10^{-14} \text{ m}^2$  and a flexural strength of approximately 35 MPa [3–10]. In addition, a uniform open pore structure and constant permeability are required.

Cement systems are not currently specified for the manufacture of porous aerostatic bearings. However, due to their high mechanical strength and high modulus of elasticity, cementitious systems are a potential low-cost material for aerostatic bearings. The main disadvantage of cement based composites is the non-uniform porous microstructure inherent to cement systems, which could limit their application. Nevertheless, the systematic pre-cast manufacture of cement composites using low water to cement ratio, a uniform compaction pressure and mono size particle distribution of aggregates may minimize the effects of a non-uniform microstructure. This paper

investigates the important physical properties, namely bulk density, porosity, pore size distribution and oxygen permeability of special composites designed for application as a porous aerostatic bearing.

## 2 Experimental

### 2.1 Composites preparation

The composites used in this work were a mix of ordinary Portland cement (OPC) and 99.98% pure silica particles. The OPC used was a Brazilian CP V ARI PLUS (ASTM Type III) and its chemical composition is shown in Table 1. The silica aggregate, originated from Minas Gerais state in Brazil, was chosen to provide high compressive strength to the final composites. During the manufacture of the composites, the parameters studied were the silica particle size, silica particle shape and uniaxial pressure level. The silica particle sizes used were 500, 250, 125 and 44  $\mu\text{m}$ , each one with a mono size particle distribution. The silica particle shape was divided into spherical and non-spherical.

Cold pressed compaction was used in this work. The compaction pressures used were 10 MPa and 30 MPa, both based on the studies of Bajza [11] and Cheeseman et al. [12] who found that these levels of pressure provide high strength ( $\sim 50 \text{ MPa}$ ) and suitable porosity levels ( $\sim 30 \text{ vol.}\%$ ) for this specific application. The water/cement ratio (w/c) of

**Table 1** Chemical analysis of OPC

Oxides	(%)
CaO	64.14
SiO <sub>2</sub>	19.45
Al <sub>2</sub> O <sub>3</sub>	4.75
Fe <sub>2</sub> O <sub>3</sub>	3.12
MgO	0.80
K <sub>2</sub> O	0.66
Na <sub>2</sub> O	0.20
SO <sub>3</sub> (%)	2.85
Loss in ignition (1000°C)	3.31
Free lime	0.67
Specific surface (Blaine)	4729 cm <sup>2</sup> /g



0.20 and silica/cement (s/c) ratio of 0.67 were constant for all composites to permit a direct comparison. The low w/c ratio chosen in this study was sufficient to ensure that no water was expelled from the samples when the cold pressed compaction pressure was applied during the manufacture of the composites.

The OPC, silica aggregates and water were mixed for 5 min using a small Hobart Mixer. Plastics tubes inside a steel die were used to manufacture the cold pressed samples with a diameter 27.62 mm. The samples were compacted for 1 min and then sealed in plastic bags to avoid desiccation. Samples were kept for 28 days at room temperature and at approximately 60% relative humidity. After curing, the samples were cut using a precision saw to ensure a constant sample height, i.e., 45.30 mm.

The combination of the parameters studied (silica size, shape and compaction pressure) led to the manufacture of 16 different composites, as shown in Table 2. A minimum of 2 replicates (Replicate 1 and Replicate 2) and a randomization principle was carried out for estimation of the experimental error and to provide a basis for analysis of the experimental results.

**Table 2** Experimental conditions

Composite	Factors/Levels		
	Size ( $\mu\text{m}$ )	Geometry	Pressure (MPa)
C1	500	Spherical	30
C2	500	Spherical	10
C3	500	Non-spherical	30
C4	500	Non-spherical	10
C5	250	Spherical	30
C6	250	Spherical	10
C7	250	Non-spherical	30
C8	250	Non-spherical	10
C9	125	Spherical	30
C10	125	Spherical	10
C11	125	Non-spherical	30
C12	125	Non-spherical	10
C13	44	Spherical	30
C14	44	Spherical	10
C15	44	Non-spherical	30
C16	44	Non-spherical	10

## 2.2 Apparent porosity and pore size distribution

Apparent porosity is a measure of the void spaces in a material, and is measured as a fraction, between 0 and 1, or as a percent between 0% and 100%. The apparent porosity was calculated by the vacuum saturation method according to the RILEM specification CPC 11.3 [13]. In this method, the samples were dried to a constant weight at 105°C and the dry weight was recorded ( $W_1$ ). The samples were subsequently saturated with water under vacuum and the saturated weight suspended in water ( $W_2$ ) and the saturated surface dry weight ( $W_3$ ) were measured. The apparent porosity was calculated using Eq. 1.

$$P_o = \frac{W_3 - W_1}{W_3 - W_2} \quad (1)$$

Three samples were used and the average of the results was expressed as the apparent porosity.

Mercury intrusion porosimetry was carried out using a Micromeritics WIN9400, which measures pores with a diameter between 0.003 and 320  $\mu\text{m}$ . Composite monoliths 28 days old were dried at 50°C for 24 h and kept in a vacuum desiccator prior to testing. The cumulative volume of pores and pore size distribution was analyzed for all 16 composites.

## 2.3 Oxygen permeability

Oxygen permeability was carried out using the Leeds permeameter described by Cabrera and Lynsdale [14]. In this method, pressurized oxygen is made to flow vertically through a sample, which is completely sealed by a rubber cylinder inside a steel cylinder. The gas flow rate is measured using a bubble flow meter and is recorded after a steady state of flow has been reached (approximately 30 min from the start of the experiment). The intrinsic permeability may be calculated by the Eq. 2 [14] and [15]:

$$k = \frac{4.04 \times 10^{-16} \times Q \times P_2 \times L}{A \times (P_1^2 - P_2^2)} \quad (2)$$

where  $k$  is the intrinsic permeability ( $\text{m}^2$ );  $L$  is the length of the specimen (m);  $A$  is the cross-sectional area of specimen ( $\text{m}^2$ );  $Q$  is the flow rate ( $\text{cm}^3/\text{s}$ );  $P_1$  is the absolute applied pressure (bar),  $P_2$  is the pressure at which the flow rate is measured, equal to 1 bar. The constant  $4.04 \times 10^{-16}$  accounts for the transformation

of units. Prior to testing, the samples were oven dried at 105°C for 24 h. Two samples were tested for each composite and the mean was reported.

#### 2.4 Dry bulk density

The dry bulk density of the composites was calculated by dividing the dry weights (after 24 h of drying at 105°C) by the volume of the samples (27.62 mm of diameter, 45.30 mm of height). The results of dry bulk density were compared with results of porosity and permeability, not only to check whether there was a good correlation between these properties but also to validate the porosity and permeability results of the composites studied.

### 3 Experimental results

The experimental data obtained in this investigation, including bulk density, apparent porosity, average pore size and permeability are summarised in Table 3, which shows the results for Replicate 1 and the Replicate 2. The average pore size has not

been statistically analysed, as only the results of Replicate 1 are available.

The analysis of variance was performed using the statistical software *Minitab 14<sup>TM</sup>*. The *P*-values (Table 4) indicate which of the effects in the system are statistically significant, based on examination of the experimental data from Replicate 1 and Replicate 2. The effect is considered to be ‘significant’ when the *P*-value is less than or equal to 0.05. A  $\alpha$ -level of 0.05 is the level of significance, which implies that there is 95% of probability of the effect being significant. The results are presented via ‘main effect’ and ‘interaction’ plots. It should be highlighted that these plots are *not* typical ‘scatter’ plots, but serve to illustrate the statistical analysis and provide the variation on the significant effects.

#### 3.1 Interaction and main effects

A ‘main effects’ plot is primarily useful when several factors such as particle size, particle shape and pressing pressure influence the property of the composite. These plots are used to compare the changes in the mean level to determine which of

**Table 3** Experimental results for Replicate 1 and Replicate 2

Composite	Replicate 1				Replicate 2		
	Bulk density (g/cm <sup>3</sup> )	Apparent porosity (%)	Permeability ( $\times 10^{-16}$ m <sup>2</sup> )	Average pore size ( $\mu$ m)	Bulk density (g/cm <sup>3</sup> )	Apparent porosity (%)	Permeability ( $\times 10^{-16}$ m <sup>2</sup> )
C1	2.376	7.31	0.82	0.0124	2.378	6.23	0.77
C2	2.366	8.40	0.89	0.0091	2.332	7.85	0.98
C3	2.356	7.91	0.97	0.0092	2.353	8.32	0.98
C4	2.331	8.92	0.69	0.0143	2.323	9.74	0.77
C5	2.318	7.99	1.03	0.0090	2.338	8.82	0.96
C6	2.321	9.93	0.79	0.0151	2.328	10.38	0.92
C7	2.347	8.11	0.75	0.0090	2.313	9.53	0.89
C8	2.285	10.13	1.44	0.0156	2.280	10.50	0.82
C9	2.242	14.48	1.86	0.0183	2.209	13.48	2.02
C10	2.199	15.61	5.68	0.0210	2.166	15.45	6.37
C11	2.239	11.23	1.17	0.0095	2.235	10.14	1.50
C12	2.202	13.62	11.51	0.0200	2.176	14.62	11.27
C13	2.147	16.03	6.16	0.0108	2.159	15.89	5.16
C14	2.105	17.55	16.37	0.0120	2.115	18.53	14.82
C15	2.068	17.03	25.98	0.0244	2.096	17.97	20.01
C16	2.020	19.77	64.54	0.0115	2.036	20.34	101.36

**Table 4** Analyses of variance (ANOVA),  $P$ -values ( $\alpha \leq 0.05$ )

Source	$P$ -values		
	Bulk density	Apparent porosity	Ln (Permeability)
Size	0.000	0.000	0.000
Geometry	0.000	0.246	0.000
Pressure	0.000	0.000	0.000
Size $\times$ Geometry	0.000	0.000	0.000
Size $\times$ Pressure	0.314	0.164	0.000
Geometry $\times$ Pressure	0.175	0.248	0.012
Size $\times$ Geometry $\times$ Pressure	0.458	0.269	0.002
Standard deviation	0.013	0.609	0.068
$R^2$ (%)	99.19	98.92	99.40

the processing factors influence the properties (the ‘response’) the most. This analysis comprises examination of the mean value for each factor and comparison of the mean value and relative strength of several factors [16, 17].

In addition to a ‘main effect’, there may also be an ‘interaction effect’. An interaction is present when the change in the mean response of a composite (e.g. bulk density) from a low to high level of a factor (e.g. particle size) also depends on the level of a second factor (e.g. particle shape). Interactions plots show the interaction effect of two or more factors (e.g. size and geometry; size, geometry and pressure) on the response and enable the comparison of the relative strength of the effects. When an interaction effect is significant, the main effects are not analyzed separately [16, 17].

### 3.1.1 Bulk density

Table 4 shows that the  $P$ -values for all three main effects of particle size, particle geometry and pressure are zero for bulk density. There was strong evidence of a significant effect of the particle size, geometry and pressing pressure on the bulk density. Only the main effect of pressure on the bulk density was considered, as there was an interaction effect of size and geometry (see Table 4, Fig. 1).

Figure 1 shows that a change from low to high pressure corresponded to an increase in the bulk densities. Such a response is typically found when cold pressed compaction is applied. The bulk density data for all the samples varied from 2.02 to 2.38 g/cm<sup>3</sup>.

The size and geometry interaction was also a significant factor, as  $P$ -value (0.000) was  $<0.05$ .

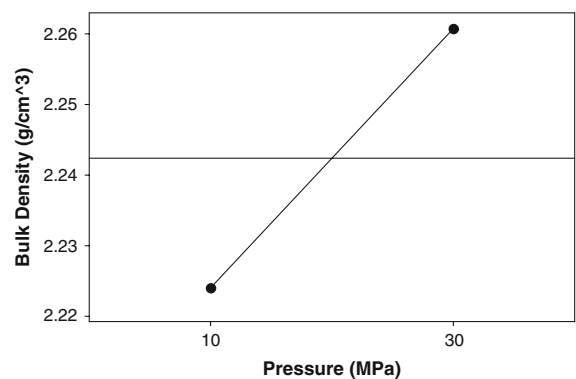
**Fig. 1** Main effect plot for bulk density, pressure

Figure 2 shows that the small 0.044 mm particles provided the lowest bulk density. The interaction plot in Fig. 2 also indicates that the bulk density decreased when the geometry of 0.044 mm silica particles changed from spherical shaped to non-spherical particles. The particle size factors of 0.500 mm and 0.250 mm particles also showed a decrease in the bulk density when using non-spherical geometry particles. However, only a small variation of bulk density between spherical and non-spherical particles was observed for a particle size factor 0.125 mm. The mean percentage difference of the bulk density between the largest and the smallest particle sizes was approximately 12%. Compared to the non-spherical particles, the spherical particles provided an increase of nearly 15% on the mean bulk density.

The  $R^2$  value represents the proportion of variation in the response data explained by the terms in the model. The  $R^2$  value given at the bottom of Table 4 (99.19%) shows that the model postulated for the bulk density measurements fitted the data well.

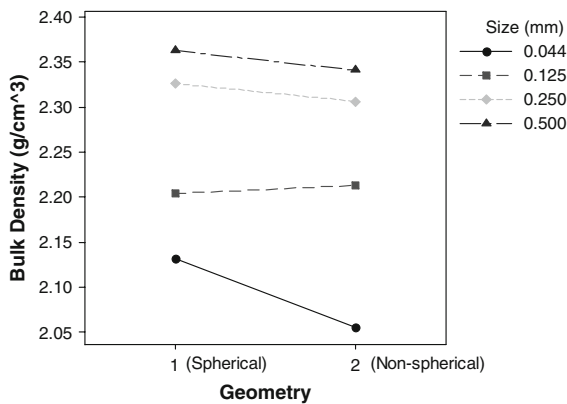


Fig. 2 Interaction plot for bulk density, size and geometry

A material used as a porous bearing should be lightweight [2–5], especially for highly dynamic applications with high accelerations, which imply that a low bulk density is desirable. The highest bulk density was reached when the experimental treatment corresponded to a large particle size, spherical shape silica and high-pressure compaction. On the other hand, the lowest bulk density was attained when the experimental treatment was a small particle size, non-spherical shape and low level of pressure (C16 in Table 1).

### 3.1.2 Apparent porosity

The apparent porosity results are presented in Table 3. The porosity data varied from 6.23% to 20.34%. Table 4 shows that the most significant factors affecting the apparent porosity were particle size, compaction pressure and the interaction factor size and geometry, since they all have  $P$ -values = 0.000 (underlined in Table 4). The  $R^2$  is 98.92%, indicating that the model postulated for the apparent porosity measurements fitted the data very well.

According to Jambor [18], there are two distinct stages in the development of pore structure in cement composites. The first stage is determined by the composition of the mixture and by its degree of compaction. The second stage is strongly influenced by the hydration process, i.e. the volume of pores decrease as hydration progresses in the composites. The main effect plot for apparent porosity (Fig. 3) shows that changing from low (10 MPa) to high (30 MPa) pressure led to a drop of  $\sim 17\%$  in the

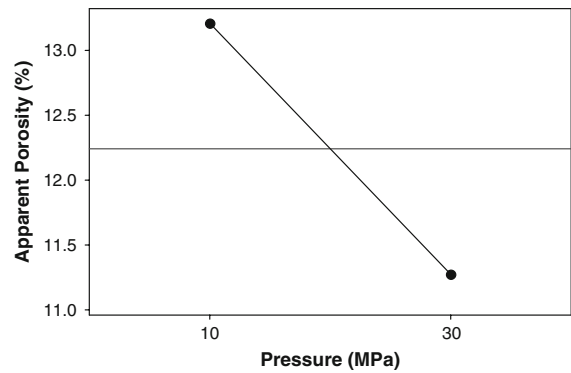


Fig. 3 Main effect plot for apparent porosity, pressure

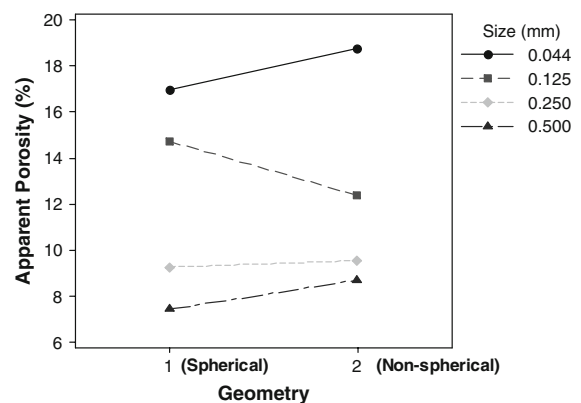


Fig. 4 Interaction plot for apparent porosity, size and geometry

mean of the apparent porosity. This indicates that high compacting pressure provided lower apparent porosity, in accordance with Jambor [18].

Figure 4 shows the interaction plot between size and geometry for apparent porosity. It is possible to observe that, apart from the silica particle size of 0.125 mm, spherical particles provided lower apparent porosities than the non-spherical geometry. These results are in accordance with the packing theory described by Mcgeary [19], which assumes that the apparent porosity of cement pastes made with spherical particles is lower than that of pastes made with non-spherical particles. The percentage difference between the values of apparent porosity for the largest and the smallest particle sizes was approximately 122%.

The apparent porosity values required for porous bearings application should be between 20% and 35% [3, 5]. The highest apparent porosities were achieved

when the cementitious composite were manufactured with small silica particles, non-spherical particles and low pressure (composite C16 in Table 1).

### 3.1.3 Pore size distribution (MIP)

The sinter ceramic developed by Kwan [3] exhibited a satisfactory pore size distribution of 0.1–1.0  $\mu\text{m}$  for application as a porous bearing. Figure 5 shows the cumulative volume of pores provided by mercury intrusion porosimetry (MIP). This graph shows that the composites made with small silica particles (44 and 125  $\mu\text{m}$ ) were characterised by a higher cumulative volume of pores (C16, C14, C13, C11). In addition, the cumulative volume of pores within the range 0.1–1.0  $\mu\text{m}$  was higher for C10, C12, C13, C14, C15 and C16, which are the composites made with silica particles with 125 and 44  $\mu\text{m}$ .

Figure 6 shows the distribution of pores for the studied composites. It is possible to note that, as the silica particle size decreased, the volume of larger pores increased. Based on the particle packing theory described by Mcgeary [19], this behaviour was not expected. In composites using the silica particles of 44  $\mu\text{m}$  in size (C13–C16, Fig. 6d), the pores size exceed 1  $\mu\text{m}$  in diameter, which is not observed for the other larger silica particles. For the large silica particles (500, 250 and 125  $\mu\text{m}$ ), the cement grains ( $\sim 44 \mu\text{m}$ ) are smaller than the silica particles and the cement is likely to pack the gaps between the large silica particles, leading to high packing. For the smallest silica particles (44  $\mu\text{m}$ ), the particle size difference between the silica and cement is reduced and the cement may not be able to

pack between the silica grains, leading to a low degree of packing. The ‘microfiller effect’ [20] is the other extreme whereby very small ( $\sim 0.1 \mu\text{m}$ ) silica fume particles are used which are much smaller than the cement grains. In this case the small silica fume particles pack into the space between cement grains, thus reducing the space available for water and producing dense structure of hydration products.

Figure 6 also indicates that for a constant silica particle size, the composites with largest pores are those made using low pressure, i.e., 10 MPa. This is in accordance with Figs. 1 and 3 for bulk density and apparent porosity, respectively. The high pressure decreases the porosity of the matrix and makes it denser, also reducing the pore sizes.

### 3.1.4 Oxygen permeability

The permeability data is presented in Table 3. The permeability results exhibit an exponential behaviour; therefore, the response of the statistical factorial analysis was presented as natural logarithms, “In (permeability)”.

The *P*-values for all three main effects in Table 4 are zero, which means that there is evidence of a significant effect of size, geometry and pressure on the composite permeability. However, only the interaction plot was analysed, as the interaction effect of size, geometry and pressure was also significant. The  $R^2$  for the curves in Fig. 10 is 99.40%, indicating that the model postulated for the permeability measurements fitted the data well.

The results in Fig. 7 are in accordance with the apparent porosity results (Figs. 3, 4), since the use large silica particle sizes, spherical geometry and high pressure gave the lowest permeability and lowest porosity results for the composites.

The possible reason for the reduced permeability in composites with large silica particles may be explained as follows. The water cement ratio used in the composites is low (0.20) and the amount of water was not sufficient to fully hydrate all the cement grains. Those composites which were able to retain water the most had better hydration and consequently higher density, strength and lower porosity and permeability. The specific surface area was lower for the largest silica particles. As a result, a thicker film of water around the large particles may have provided a better hydrating process, as well as the lowest permeability and highest strength.

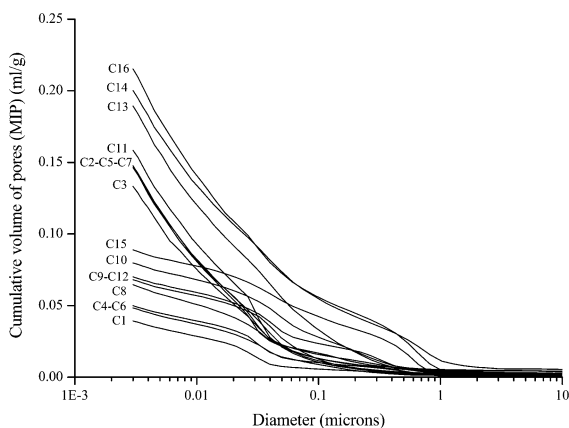


**Fig. 5** Cumulative volume of pores for the composites studied

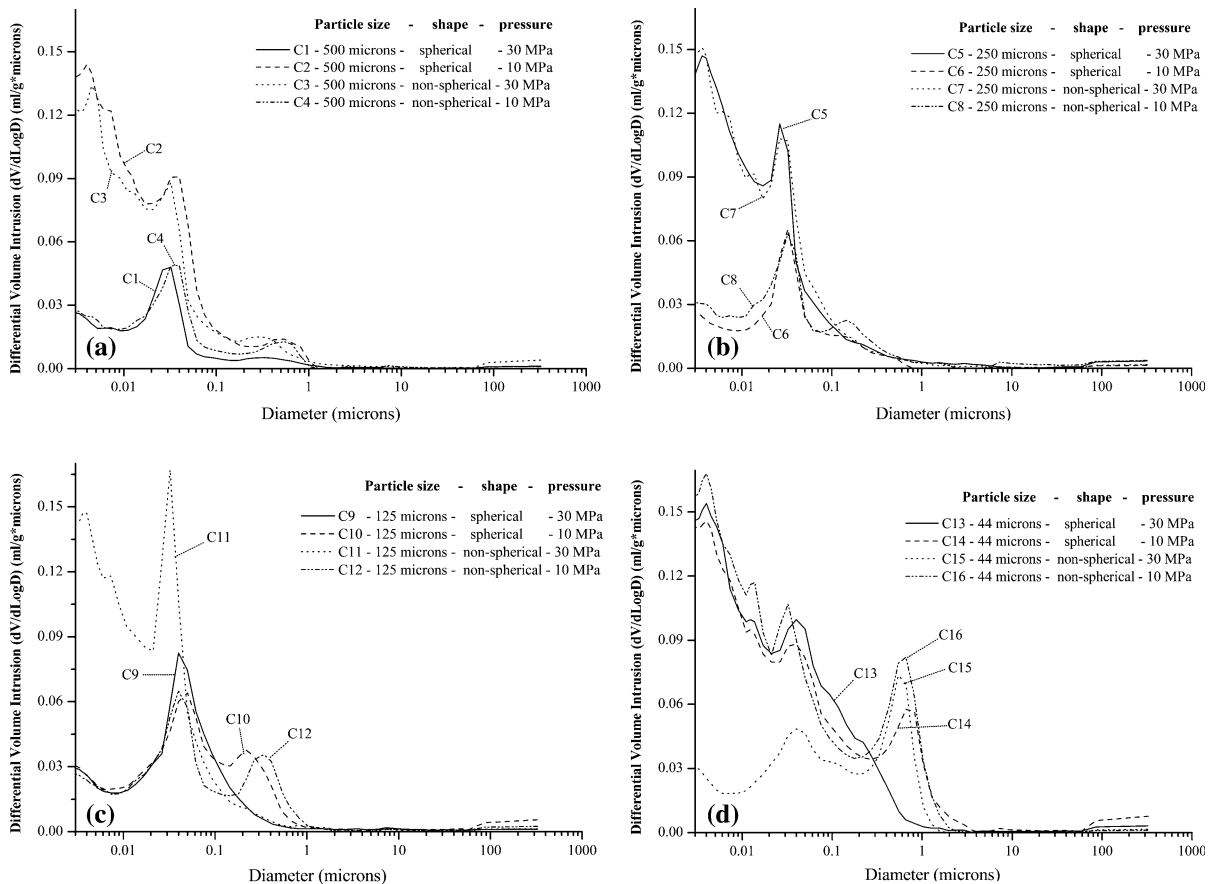


**Fig. 6** Pore size distribution for the composites studied

According to the authors [3–10], the permeability coefficient required for porous bearings application should range from  $3.1 \times 10^{-15}$  to  $8.4 \times 10^{-14} \text{ m}^2$ . The permeability of the composites studied varied from  $7.7 \times 10^{-17}$  to  $10.14 \times 10^{-15} \text{ m}^2$ , indicating that the composites C14, C15 and C16 (Table 2) have the permeability requirements to be applied as porous bearings.

The following section will now describe the correlation between responses so that the composite parameters may be chosen to provide tailored properties.

### 3.2 Correlation between responses

#### 3.2.1 Apparent porosity and permeability

The scatter plot in Fig. 8 shows the relationship between apparent porosity and permeability. A potential regression obtained from Eq. 3, with  $R^2 = 86.21\%$ , reveals a significant correlation

between these properties, where  $P_o$  is the apparent porosity and  $P_e$  is the permeability.

$$P_e = 0.0648e^{0.3012P_o} \quad (3)$$

A number of mathematical models [21–24] have been developed in an attempt to predict the permeability coefficient as a function of apparent porosity or other properties. This relevant correlation not only confirms the existence of this relation between these properties, but also provides a new equation to predict the permeability, which is a property that is generally more difficult to measure than porosity.

#### 3.2.2 Apparent porosity and bulk density

Figure 9 shows the correlation between the bulk density and the apparent porosity of the composites. There is a linear correlation between these variables represented by the Eq. 4 with  $R^2 = 96.70\%$ , where  $P_o$  is the apparent porosity and  $\rho$  the bulk density.

**Fig. 7** Interaction effect plot for  $\ln$  (permeability), size, geometry and pressure

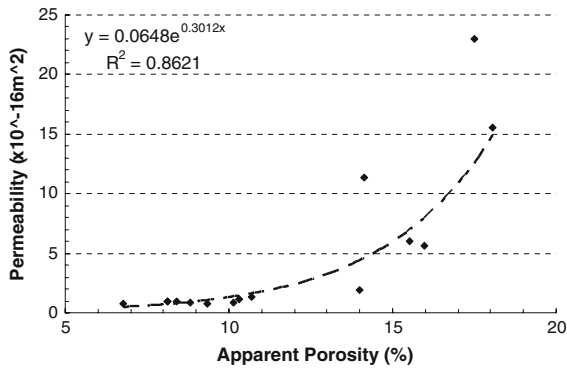
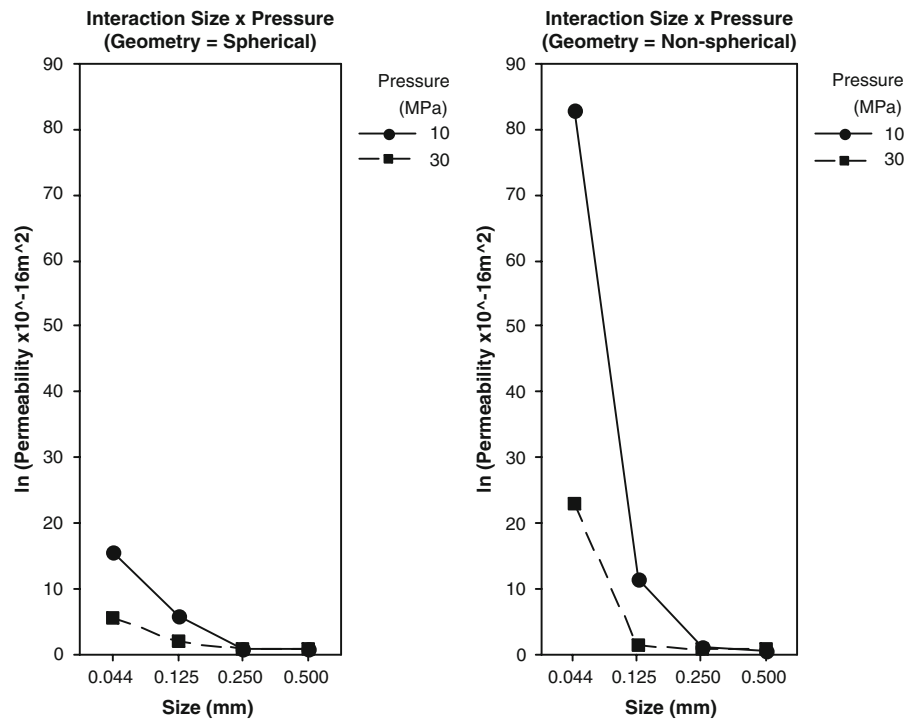


**Fig. 8** Correlation between apparent porosity and permeability

This correlation shows that the smaller the apparent porosity the bigger the bulk density of the cementitious composites.

$$P_o = -37.943\rho + 97.331 \tag{4}$$

### 3.2.3 Permeability and bulk density

Figure 10 reveals a significant correlation between the bulk density ( $\rho$ ) and permeability ( $P_e$ ), which can be represented by the Eq. 5 with  $R^2 = 91.85\%$ . It was confirmed that an increase in the bulk density corresponds to a drop in the oxygen permeability.

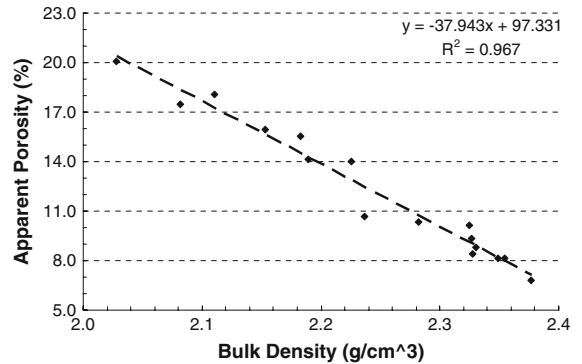


**Fig. 9** Correlation plot between the bulk density and the apparent porosity

$$P_e = -1142\rho^3 + 8033.6\rho^2 - 18840\rho + 14729 \tag{5}$$

It is possible to obtain another equation to estimate the permeability as a function of bulk density, by substituting Eq. 4 in Eq. 3. Then, Eq. 6 with  $R^2 = 81.88\%$  can be deduced:

$$P_e = 0.0648e^{(0.3012 \cdot (-37.943\rho + 97.331))} \tag{6}$$

The correlation equations between the bulk density, apparent porosity and permeability provide a method for determining the gas permeability of the



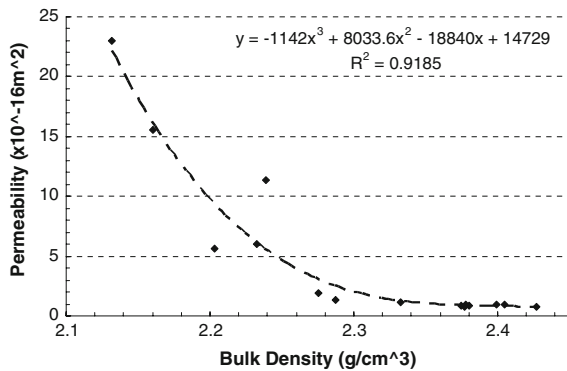


**Fig. 10** Correlation plot between the bulk density and the permeability coefficient

composites and can help the continuous development of new cementitious composites designed for porous bearings.

#### 4 Conclusions

A design of experiments and full factorial analysis has been used to analyze and develop cementitious materials for aerostatic bearings with low bulk density, high permeability coefficient and high porosity. A central composite design can be adopted in future research in order to investigate the nonlinear effect of the factors.

The main conclusions from this paper are:

- (i) Compaction pressure and the correct selection of the particle size and geometry optimize the particle packing. The main factors influencing the composite bulk density are particle size, particle geometry and compaction pressure. The highest bulk density was achieved when the composites are made with large particle size (0.500 mm), spherical particle shape and high compaction pressure (30 MPa).
- (ii) Silica particle size and pressure were significant factors affecting the apparent porosity. The highest apparent porosity, which is required for porous bearings, was achieved when the composite was manufactured with small silica particles (0.044 mm) and lower compaction pressure (10 MPa). The interaction effect of size and geometry was also significant, showing that small particles give rise to larger apparent porosities, especially when non-spherical geometry of silica particles is used.

- (iii) The pore size distribution was in accordance with the apparent porosity results, i.e. small silica particles gave rise to higher porosity composites. When the silica particle size was constant, the composites with the larger pores were those made with lower pressure, i.e., 10 MPa.
- (iv) Permeability was significantly influenced by the combination of the factors particle size, geometry and pressure. The highest permeability was achieved when the composite was made with small silica particles (0.044 mm), non-spherical geometry and low level of pressure (10 MPa).
- (v) The scatter graphics have revealed significant correlations between the bulk density, apparent porosity and permeability coefficient. Although the precise values of the constants in the equations may change for particular cement systems, the equations provided by the mathematical regressions are a valuable tool to determine the permeability coefficient from the bulk density or apparent porosity results.

The composites C14 and C15, made with 0.044 mm non-spherical silica particles, as well as the composite C16, made with 0.044 mm spherical silica particles with low pressure (10 MPa) have the structure and properties required for the manufacture of porous aerostatic bearings. These composites are promising materials on the application of cementitious composites for aerostatic bearing applications.

**Acknowledgements** The authors would like to thank the Department of Mechanical Engineering at the University of Bath, UK, and also the Department of Civil and Structural Engineering at the University of Sheffield, UK, for their support with the laboratory techniques. This project was funded by Capes, the Brazilian Ministry of Education Agency, to which the authors would also like to acknowledge.

#### References

1. Cheng K, Rowe WB (1995) A selection strategy for the design of externally pressurized journal bearings. *Tribol Int* 28:465–474. doi:10.1016/0301-679X(95)00011-R
2. Slocum A (1992) *Precision machine design*. Prentice Hall, New Jersey
3. Kwan YBP, Corbett J (1998) Porous aerostatic bearings—an update review. *Wear* 222:69–73. doi:10.1016/S0043-1648(98)00285-3

4. Fourka M, Bonis M (1997) Comparison between externally pressurized gas thrust bearings with different orifice and porous feeding system. *Wear* 210:311–317. doi:[10.1016/S0043-1648\(97\)00079-3](https://doi.org/10.1016/S0043-1648(97)00079-3)
5. Majumdar BC (1980) Externally pressurised gas bearings: a review. *Wear* 62:299–314. doi:[10.1016/0043-1648\(80\)90175-1](https://doi.org/10.1016/0043-1648(80)90175-1)
6. Gargiulo EP, Gilmour PW (1968) A numerical solution for the design of externally pressurised porous gas bearings: thrust bearings. *J Lubrif Technol Trans ASME Oct.*: 810–817
7. Murti PRK (1976) Analysis of externally pressurised gas porous bearings. *J Lubrif Technol Trans ASME* 43:404–408
8. Polone J, Goret R (1980) The use of ground material in gas lubrication. *Wear* 60:349–356. doi:[10.1016/0043-1648\(80\)90233-1](https://doi.org/10.1016/0043-1648(80)90233-1)
9. Kwan YBP, Corbett J (1998) Slip inertia effects in porous aerostatic bearings. *Tribol Int* 31:779–786. doi:[10.1016/S0301-679X\(98\)00101-7](https://doi.org/10.1016/S0301-679X(98)00101-7)
10. Stout KJ, Barrans SM (2000) The design of aerostatic bearings for application to nanometre resolution manufacturing machine systems. *Tribol Int* 33:803–809. doi:[10.1016/S0301-679X\(00\)00118-3](https://doi.org/10.1016/S0301-679X(00)00118-3)
11. Bajza A (1983) Structure of compacted cement pastes. *Cement Concr Res* 13:239–245. doi:[10.1016/0008-8846\(83\)90107-2](https://doi.org/10.1016/0008-8846(83)90107-2)
12. Cheeseman CR, Asavapisit S, Knight J (1998) Effect of uniaxial pressing ordinary Portland cement pastes containing metal hydroxides on porosity, density and leaching. *Cement Concr Res* 28:1639–1653. doi:[10.1016/S0008-8846\(98\)00143-4](https://doi.org/10.1016/S0008-8846(98)00143-4)
13. Recommendations of RILEM (1979) CPC 11.3: absorption of water by immersion under vacuum. June 1979
14. Cabrera JG, Lynsdale CJ (1988) A new gas permeameter for measuring the permeability of mortar and concrete. *Mag Concr Res* 40:177–182
15. Cabrera JG, Claisse PA (1999) Oxygen and water vapour transport in cement-silica fume pastes. *Constr Build Mater* 13:405–414. doi:[10.1016/S0950-0618\(99\)00039-2](https://doi.org/10.1016/S0950-0618(99)00039-2)
16. Jeff Wu CF, Hamada M (2000) *Experiments: planning, analysis and parameter optimization*. Wiley, New York
17. Montgomery DC (1997) *Introduction to statistical quality control*. Wiley, New York
18. Jambor J (1990) Pore structure and strength development of cement composites. *Cement Concr Res* 20:948–954. doi:[10.1016/0008-8846\(90\)90058-6](https://doi.org/10.1016/0008-8846(90)90058-6)
19. Mcgeary RK (1961) Mechanical packing of spherical particles. *Am Ceram Soc J* 44:513–522. doi:[10.1111/j.1151-2916.1961.tb13716.x](https://doi.org/10.1111/j.1151-2916.1961.tb13716.x)
20. Nehdi M, Mindess S, Aitcin PC (1998) Rheology of high-performance concrete: effect of ultrafine particles. *Cement Concr Res* 28:687–697. doi:[10.1016/S0008-8846\(98\)00022-2](https://doi.org/10.1016/S0008-8846(98)00022-2)
21. Robinson AT (1964) Permeability of tungsten matrices as a function of density, particle size and shape. *Trans ASM* 57:650–657
22. Cliffel EM Jr, Smith WE, Schwope AD (1966) Theory and applications of controlled permeability. *Mod Dev Powder Met* 3:114–128
23. German RM (1981) Porosity and particle size effects on the gas flow characteristics of porous metal. *Powder Technol* 30:81–86. doi:[10.1016/0032-5910\(81\)85029-2](https://doi.org/10.1016/0032-5910(81)85029-2)
24. Smith DW, Marth T (1980) An examination of the effects of pore morphology on gas flow through sintered compacts. *Mod Dev Power Met* 12:835–854